Journal of Materials Chemistry B

ROYAL SOCIETY OF CHEMISTRY

PAPER

View Article Online
View Journal

Cite this: DOI: 10.1039/d0tb01647k

Block copolymer [(L-GluA-5-BE)-*b*-(L-AspA-4-BE)]-based nanoflower capsules with thermosensitive morphology and pH-responsive drug release for cancer therapy†

Chander Amgoth, *[a] Shuai Chen,[a] Tirupathi Malavath[b] and Guping Tang *[a]

Herein, the synthesis of an amino-acid-based di-block copolymer (di-BCP) in-between an L-glutamic acid-5-benzyl ester and L-aspartic acid-4-benzyl ester [(L-GluA-5-BE)-*b*-(L-AspA-4-BE)] has been reported. However, the synthesis of di-BCP of [(L-GluA-5-BE)-*b*-(L-AspA-4-BE)] was carried out through the facile modified ring-opening polymerization (ROP) without using any surfactants and harmful chemicals. Interestingly, the synthesized [(L-GluA-5-BE)-*b*-(L-AspA-4-BE)] has been used to design nanoflower capsules (NFCs) with surface-functionalized nanoflakes and petals. Notably, the simple solvent propanol has been used as a dispersing medium for the di-BCP-based powder to observe morphology of NFCs. Moreover, these amino-acid-based NFCs are biocompatible, biodegradable, and bio-safe for mankind usage. Consequently, di-BCP-based NFCs show changes in morphology with different temperature conditions, *i.e.*, at ~10 °C, ~25 °C (RT), and ~37 °C (body temperature). Furthermore, the average thickness of the surface-functionalized nanopetals has been calculated as ~324 nm (in diameter). Similarly, the average distance between petals is calculated as 3.6 μm and the pore depth is ~21 nm. Additionally, the porosity throughout the surface of capsules in-between nanopetals is an advantageous characteristic feature to improve the drug/paclitaxel (PTX) loading capacity. It is a unique and novel approach to design NFCs, which are a potential payload for nanomedicine and cancer therapy. Furthermore, NFCs were used to evaluate the loading efficacy of drugs and showed ~78% (wt/wt%) of the PTX loading. Moreover, NFCs showed ~74% drug release at physiological body temperature. Thus, NFCs showed remarkable release at acidic pH medium. However, PTX released from NFCs showed greater cell inhibition (*i.e.*, ~79%) with an increase of the PTX concentration after 24 h incubation over HeLa (human epithelial cervical cancer) cells. Besides, PTX released from NFC showed significant (~34%) cell killing capacity. Such promising NFCs are recommended for breast, liver, and lung cancer therapeutics.

Received 3rd July 2020,
Accepted 20th August 2020

DOI: 10.1039/d0tb01647k

rsc.li/materials-b

Introduction

The design and development of amino-acid-based surface-functionalized NFCs with porosity and nanopetals for enhanced drug loading and targeted release kinetics are an essential task for cancer therapy.[1] However, material science and engineering, followed by the combination of life sciences, can fulfill the research area (such as drug delivery and cancer theranostics) with potential amino-acid-based carrier capsules. The characteristic properties of block copolymers (BCPs) such as low density, low molecular weight, self-assembly nature, amphiphilic (hydrophobic and hydrophilic) nature, cross-linking and easy branching capability followed by the net-work formation led to the synthesis of the di-BCP of [(L-GluA-5-BE)-*b*-(L-AspA-4-BE)], as explained by Amgoth *et al.*[2] The self-assembly mechanism through the coordinative conjugation between two or more different polymers leads to the formation of BCPs. Therefore, biocompatible, biodegradable, and bio-safe polymers with active functional groups play a crucial role in synthesizing BCPs, followed by the design and development of surface-functionalized nanoarchitectured materials (such as capsules and particles).[3] However, BCPs have an enormous potential for use in the design and development of carrier capsules with surface-functionalized properties such as smooth and rough surface, porosity, fringes, and nanopetals.[4] Interestingly, such bio-inspired materials play a vital role in order to evaluate the bio/pharmaceutical applications, especially for cancer treatment. The systemic research on amino-acid-based BCPs *via* supra-molecular hydrophobic imprinting helps in the design

[a] *Department of Chemistry, Zhejiang University, Hangzhou-310028, China. E-mail: tangguping@zju.edu.cn*
[b] *Department of Biochemistry and Molecular Biology, Tel Aviv University, Israel*
† Electronic supplementary information (ESI) available. See DOI: 10.1039/d0tb01647k

of potential surface-functionalized nanomaterials, which can be recommended for drug/cell/gene delivery systems.[5] BCPs are often referred to as wonder and magic polymers for drug delivery and cancer therapy because of their precise control over the polymer length, size scale, chain network, branching capacity, easy changeability in shape, and morphology without using any harmful chemicals.[6] Several factors certainly affect the properties of the polymer nanomaterials, such as solvent, temperature conditions, reaction methods, purity, environment, concentration, pH of the medium, stirring and sonication methods.[7] Li *et al.* reported on the polysaccharides and dual-drug response for conjugated cancer chemotherapy.[8] Similarly, different fullerene-type capsules, porous metal–organics, hydrogels, mesoporous metal–organic frameworks, aggregates, organic cages, and composite frameworks were also recommended as promising drug delivery systems by Wu *et al.*[9] and Wang *et al.*[10,11] Ding *et al.* reported on the engineered nanomedicine for enhanced tumor penetration through the translational advanced strategies for chemotherapy and the role of materials.[12] All of these carrier materials have certain limitations for their use in bio/pharmaceutical applications. These limitations include low loading capacity, burst release, side effects, cytotoxicity, biocompatibility, biodegradability, biosafety, size, shape and morphology. Such limitations can be addressed through the amino-acid-based BCPs with advanced characteristic features like porosity, larger specific surface area, ideal particle size, shape, and time-to-time tunable properties for cancer therapeutics.[10–13] Biodegradable polymers conjugated with amino-acids attracted interest in the synthesis of di-BCP of [(L-GluA-5-BE)-*b*-(L-AspA-4-BE)], followed by the design and development of thermosensitive and pH-responsive NFCs. Herein, the synthesis of amino-acid-based di-BCP of [(L-GluA-5-BE)-*b*-(L-AspA-4-BE)], followed by the design and development of surface-functionalized NFCs, has been deliberated. The formula and chemical structure of amino-acid-based polymers, L-GluA-5-BE and L-AspA-4-BE, differ only by a methyl ($-CH_2-$) group, which is excess in L-GluA-5-BE, but their self-assembly and formulation of NFCs are amazing for mankind usages.[14–16] L-GluA-5-BE and L-AspA-4-BE both have greater affinity in acidic environments. The acidic medium (pH = 4 and lower than 4) leads to a change in the protons from an acid group to amine. Since L-GluA-5-BE and L-AspA-4-BE have amine and carboxyl groups, the amine ($-NH_2$) group can gain a proton and the carboxyl/acid (–COOH) group can lose a proton at the same time under acidic pH conditions. This protonation property could be the reason for the pH-responsive nature of synthesized NFCs. The peculiar properties of L-AspA-4-BE and L-GluA-5-BE, such as aspartate and glutamate transamidation followed by the interconversion of oxaloacetate, and the donation of a nitrogen atom for other biosynthetic products help in the morphological changes with respect to various temperatures. However, water retention and nitrogen uptake can also be considerable properties for the thermosensitive morphological changes of NFCs. Nanoparticles and capsules with size ranges of 100 to 200 nm are much more suitable for targeted drug delivery, as reported by Zhao *et al.*[15] and Ge *et al.*[17] Inherently, di-BCPs of [(L-GluA-5-BE)-*b*-(L-AspA-4-BE)] are a unique and novel approach to design NFCs with adjuvant nanoarchitectured features to uplift the drug delivery issues associated with cancer therapy. The main aim of this work is to develop efficient cargo capsules for the targeted release of molecular therapeutic agents. NFCs with thermosensitive and pH-responsive characteristics are also an advantageous property for cancer therapeutics.[4–8] However, such qualitative amino-acid-based NFCs are promising drug carrier systems for various cancer treatments, such as breast, lung, liver and prostate cancers.[14,17]

Materials and methods

Materials

As per the animal ethical committee and user permit guidelines of Zhejiang University, China (Ethics code no: ZJU2010-1-01-20Y), healthy and well-cultured 4–6 week-old grown rats were purchased from the Jackson Laboratory and used for *in vivo* inflammation studies. All of the experiments related to *in vitro* and *in vivo* studies were performed according to compliance with the relevant laws and institutional user guidelines. The committee has approved all of the experiments. Furthermore, the chemicals required for the synthesis of di-BCP of [(L-GluA-5-BE)-*b*-(L-AspA-4-BE)] and the development of [(L-GluA-5-BE)-*b*-(L-AspA-4-BE)]-based NFCs were purchased with high purity, and used without further purification (except tetrahydrofuran/THF solvent). L-Glutamic acid-5-benzyl ester (>99%, Sigma Aldrich), ammonium hydroxide (NH_4OH, >98%, Sigma Aldrich), L-aspartic acid-4-benzyl ester (>99%, Sigma Aldrich), triphosgene (>99%, Sigma Aldrich), sodium citrate, (>99.8%, Sigma Aldrich), ethanol (CH_3CH_2OH, >98.5%), propanol (>97%, SDFCL), THF solvent (>98%, Merck), THF distillation condenser, THF reflux mantle, three-neck round bottom (RB) flask (1 Lt), water circulation pump, Whatmann filter paper, pH meter, conical flask, beakers, MTT (methyl thiazole tetrazolium, >99.9%, Sigma Aldrich), magnetic beads, magnetic stirrer-cum hot plate, micropipettes, 96-well plates, sample viols, centrifuge tubes, aluminium foil, HeLa cells, media for cell culture (RPMI), CO_2 incubator, orbital shaker, dd-H_2O, goggles, mask, gloves, apron, liquid N_2 container, Petri dish, ultra-sonic bath, FITC (Fluorescence isothiocyanate; >98%, Sigma Aldrich), rhodamine-B (>96%, Sigma Aldrich), DAPI ((2-(4-aminophenyl)-1*H*-indole-6-carboxamidine); >98%, Sigma Aldrich), paclitaxel (>99%, Sigma Aldrich).

Synthesis of [(L-GluA-5-BE)-*b*-(L-AspA-4-BE)]

The synthesis of di-BCP of [(L-GluA-5-BE)-*b*-(L-AspA-4-BE)] was carried out through the facile modified ring-opening polymerization (ROP) method. The oxidation reaction of L-glutamic acid-5-benzyl ester and L-aspartic acid-4-benzyl ester with the help of triphosgene leads to the formation of *N*-carboxy anhydride (NCA) or cyclic anhydride. During the oxidation reaction, the acid group of L-glutamic acid-5-benzyl ester and L-aspartic acid-4-benzyl ester were converted into NCA, which further helps in the ROP reaction. However, Fig. 1, 2 and Fig. S1 (S; ESI†) show

the steps involved in the synthesis of di-BCP and the development of NFCs at different temperature conditions. Fig. S2 (ESI†) depicts the structure of L-glutamic acid-5-benzyl ester and L-aspartic acid-4-benzyl ester, along with their NCA structures. Initially, ~2.5 g of L-glutamic acid-5-benzyl ester and L-aspartic acid-4-benzyl ester were mixed with ~1.5 g of oxidizing agent (Triphosgene), and the reactions were performed with ~50 mL of dry THF solvent followed by stirring for 1 h at ~50 °C. The resultant NCA of both acids was used for the synthesis of di-BCP of [(L-GluA-5-BE)-*b*-(L-AspA-4-BE)]. Furthermore, in a 150 mL RB flask, ~2.5 g of L-glutamic acid-5-benzyl ester was taken, and it was added to ~50 mL of dry THF solvent. Similarly, in an RB flask, ~2.5 g of L-aspartic acid-4-benzyl ester was added to ~50 mL of dry THF solvent. Both were individually allowed to stir for 30 min at room temperature (RT). Then, both dissolved mixtures were transferred into a 250 mL RB flask and added to ~2.5 g of Pd/C (activated charcoal). The neck of the RB was tightened with an H_2 gas bladder, and stirring was continued for 4 h at ~70 °C (Fig. 1, 2 and Fig. S1, ESI†). However, upon continuous stirring, the transparent solution changed into a white precipitate of [(L-GluA-5-BE)-*b*-(L-AspA-4-BE)]. After completion of the 4 h reaction, the remaining solvent was decanted, and the final [(L-GluA-5-BE)-*b*-(L-AspA-4-BE)] compound was freeze-dried under reduced pressure (50 bar, C-Gen Biotech, −80 °C freeze dryer model). The lyophilized [(L-GluA-5-BE)-*b*-(L-AspA-4-BE)] compound was allowed to dry at RT for 24 h. The compound of [(L-GluA-5-BE)-*b*-(L-AspA-4-BE)] was obtained and used for calculation of the final yield, which is ~3.6/5 g (wt/wt), *i.e.*, equal to ~72%, as explained by Amgoth *et al.*[2,4,6,11,14] and Ge *et al.*[17]

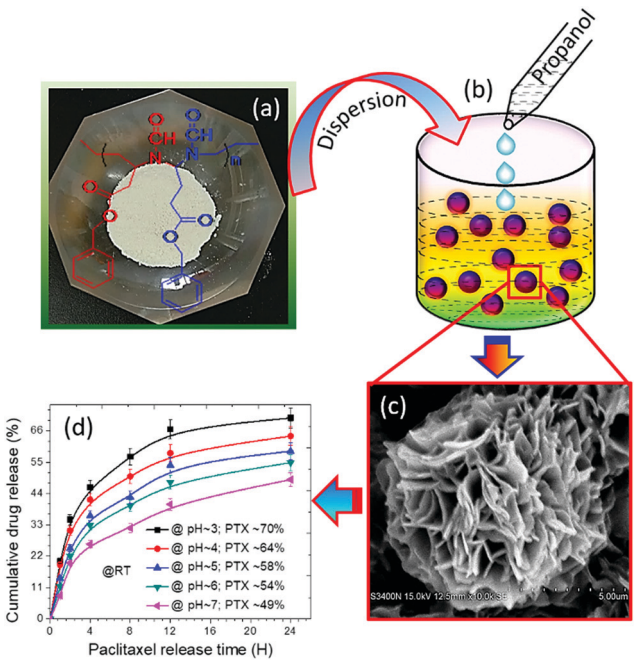

Fig. 1 Schematic illustration of the steps involved in the synthesis of di-BCP of [(L-GluA-5-BE)-*b*-(L-AspA-4-BE)], followed by the design and development of NFCs and pH-based drug release at room temperature conditions.

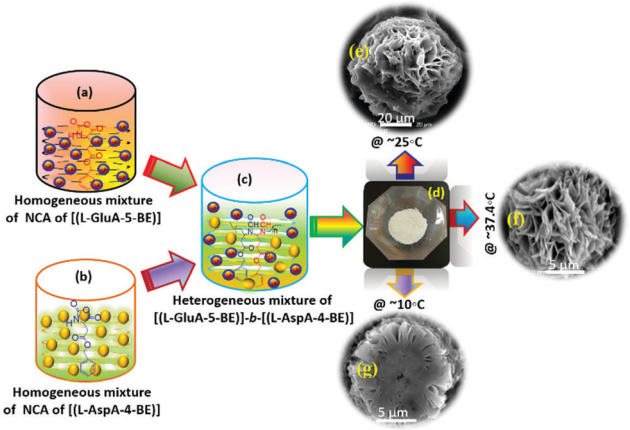

Fig. 2 Schematic (a) for NCA of L-GluA-5-BE, (b) for NCA of L-AspA-4-BE, (c) for a mixture of di-BCP of [(L-GluA-5-BE)-*b*-(L-AspA-4-BE)], (d) for the well-dried powder, (e) NFC developed at RT, (f) for NFC at body temperature, and (g) for NFC at low temperatures.

Cell culture

The human epithelia cervical carcinoma cancer cell line (HeLa) was grown in RPMI medium supplemented with 10% heat inactivated fetal bovine serum (FBS), 100 IU mL^{-1} penicillin, 100 μg mL^{-1} streptomycin and 2 mM of L-glutamine, and maintained in a humidified atmosphere with 5% CO_2 at ~37 °C. Cells were sub-cultured once every three days. The anticancer drug (PTX) was used for the treatment. PTX was dissolved in dimethyl sulfoxide (DMSO) solvent and used to load inside the NFCs. However, treatments were started with a bulk number of cells (~4×10^4 cells $well^{-1}$) in 60 mm Petri dishes, and continued with a stepwise increase in the concentrations, *i.e.*, 1.0, 5.0, 10, 15, 20, and 25 μg mL^{-1}. The inhibition of the HeLa cells with the formulations was studied with a multimode (plate) reader using 96-well plates.

MTT assay

The MTT assay is a colorimetric method to measure the activity of enzymes in living cells to reduce MTT to purple formazan crystals/dyes. Upon addition to cells, it gives purple formazan crystals. The MTT assay was basically used to determine cell viability, cell inhibition and cytotoxicity of potential medicines and our developed NFCs. MTT (3-(4,5-dimethylthiazol-2-yl)-2,5-diphenyltetrazolium bromide) is a complex chemical dye, which is widely used to stain cells during treatment with DPBS buffer solution. In a 96-well plate, ~4×10^4 cells per well were cultured and added with formulation concentrations of 1.0, 5.0, 10, 15, 20, and 25 μg mL^{-1}, respectively. However, 6-wells in a 96-well plate were kept blank and considered as the control, which means that the cells were maintained as cultured. The developed nanoformulations [(NFCs)–(PTX)–(HeLa cells)] were added to the rest of the wells, and incubated at ~37 °C in 5% CO_2 overnight. During the incubation, drug (PTX) molecules came out from the NFCs and interacted with the HeLa cells. However, the calculated amount of NFCs of ([[(L-GluA-5-BE)-*b*-(L-AspA-4-BE)]) was dispersed in propanol, and then

added to each well for thorough mixing with media (150 rpm for 4 min). The well plates were further incubated at ~37 °C in 5% CO_2 for 24 h to allow the PTX to show an effect on the cancer cells. To those wells, 20 μL of MTT solution was added and stirred at 150 RPM for ~4 min to thoroughly mix the MTT with the media. Furthermore, the plates were incubated for 24 h to allow the MTT to be metabolized with HeLa cells. The excess and unwanted residue of media was removed. The plates were used to read the optical density at 560 nm, and subtract the background at 670 nm. The optical density was directly correlated with the cell quantity, and the obtained results were used to calculate the cell viability and inhibition.

Sample preparation for SEM and AFM imaging

For the freeze-dried compound of [(L-GluA-5-BE)-*b*-(L-AspA-4-BE)], ~0.5 g was dispersed in ~1000 μL of propanol. Therefore, the well-dispersed [(L-GluA-5-BE)-*b*-(L-AspA-4-BE)] in a volume of 300 μL was separated into a cryo sample vial, and further used for ultra-sonication for 8 minutes at RT. Furthermore, the sonicated sample was divided into three parts (samples 1, 2 and 3) at 100 μL each. A 100 μL sample was kept in an ice-bath (temperature maintained at ~10 °C), the second one was maintained at room temperature (*i.e.*, ~25 °C), and the third one was maintained at body temperature (*i.e.*, ~37.4 °C). Finally, all three samples were used for the sample preparation for various microscopic characterizations, such as SEM and AFM imaging for morphological observations. However, the propanol-dispersed final compound (~20 μL) was drop-casted onto the surface of a clean and neat piece of glass, and allowed to dry at RT for 24 h. Since the polymer samples are non-conducting in nature, they were sputter-coated with metal (Au) ions before the SEM imaging. Similarly, a well-dispersed [(L-GluA-5-BE)-*b*-(L-AspA-4-BE)] solution of ~20 μL was drop-casted onto the surface of the mica sheet, and allowed to dry at RT for 24 h. The samples without any sputter coating were loaded for AFM imaging.

Results and discussion

Morphology of [(L-GluA-5-BE)-*b*-(L-AspA-4-BE)]-based nanoflower capsules

Fig. 1, 2 and Fig. S1 (ESI†) illustrate the steps involved in the synthesis of the AB-type di-block copolymer (di-BCP) of [(L-GluA-5-BE)-*b*-(L-AspA-4-BE)] through the facile modified ring-opening polymerization reactions.

Fig. 2(a and b) corresponds to NCA of L-GluA-5-BE and L-AspA-4-BE, and (c) shows the di-BCP of [(L-GluA-5-BE)-*b*-(L-AspA-4-BE)] synthesized with the help of Pd/C (palladium activated charcoal) and continuous purging of hydrogen (H_2) gas, followed by stirring with dry THF solvent at ~70 °C for 4 h.[2,8,12–17] The conversion of the acid group of L-GluA-5-BE and L-AspA-4-BE into NCA was carried out with the help of triphosgene as a strong oxidizing agent (Fig. S2, ESI†). The NCA-converted L-GluA-5-BE and L-AspA-4-BE were further used for the synthesis of di-BCP of [(L-GluA-5-BE)-*b*-(L-AspA-4-BE)] (Fig. 1, 2 and Fig. S2, ESI†), as reported by Amgoth *et al.*[2,14] and Ge *et al.*[17] Fig. S4 and S5 (ESI†) gives details about the synthesis of di-BCP of [(L-GluA-5-BE)-*b*-(L-AspA-4-BE)] and its structural confirmation through the primary characterizations, such as FTIR and ^{1}H NMR. Since the NCA of both L-GluA-5-BE and L-AspA-4-BE are structurally identical, they gave identical peak positions in FTIR and ^{1}H NMR (Fig. S4 and S5, ESI†). L-GluA-5-BE and L-AspA-4-BE differ *via* the additional methyl (–CH_2–) group in L-GluA-5-BE (Fig. 1, 2 and Fig. S1–S5, ESI†).

However, FTIR characterization for the NCA of L-GluA-5-BE and L-AspA-4-BE was performed through the KBr pellet method.[2,18] Fig. S4(a) (ESI†) corresponds to the reaction between L-GluA-5-BE, followed by the conversion of NCA of L-GluA-5-BE. Fig. S4(b) (ESI†) corresponds to the FTIR for L-GluA-5-BE. Its peak positions at ~3300 cm^{-1} (±10) correspond to the free hydroxyl (–OH) group, and those at ~3059 cm^{-1} (±10) and ~2927 cm^{-1} (±10) correspond to an asymmetric and symmetric stretch of the methyl (–CH_2–) groups, respectively. The peak positions at ~1958 and ~1872 cm^{-1} (±10) correspond to the NCA of L-GluA-5-BE. However, the peak position at ~1744 cm^{-1} (±10) corresponds to an ester (R–COO–R). The peaks at 1616, 1514, 1156, 967, and 690 cm^{-1} (±10) correspond to the complex aromatic structure of L-GluA-5-BE. Interestingly, identical FTIR peak positions and values were observed for L-AspA-4-BE in Fig. S5(b) (ESI†).[18] Furthermore, ^{1}H NMR characterization was performed for L-AspA-4-BE. The peak position (chemical shift, δ) values (nature of proton) were appended as follows: δ value at ~0.9 and 1.3 ppm, which correspond to the methyl (–CH_2–) group of benzyl, 1.9 and 2.6 ppm for the protons adjacent to the ester group, a sharp peak at 3.8 ppm corresponds to the amide (–NH) bound proton, another sharp peak at 7.26 ppm corresponds to the reference solvent $CDCl_3$ used for ^{1}H NMR characterization, and the peak position at 8 ppm belongs to the aromatic benzene ring, as shown in Fig. S4(c) (ESI†).

Furthermore, identical ^{1}H NMR peak position values were observed for L-AspA-4-BE in Fig. S5(c) (ESI†).[2,18,19] The NCA-converted L-GluA-5-BE and L-AspA-4-BE further underwent the ring-opening polymerization with palladium activated charcoal (Pd/C-10%) with the help of the continuous purge of hydrogen gas in the presence of dry THF solvent. Finally, the synthesized di-BCP of [(L-GluA-5-BE)-*b*-(L-AspA-4-BE)] was confirmed through FTIR and ^{1}H NMR characterizations, as shown in Fig. S3 (ESI†).

The final di-BCP compound was dispersed in propanol and separated into three samples. Sample 1 was stored at low temperatures (*i.e.*, maintained at ~10 °C with the help of an ice-bath), sample 2 was stored at room temperature/RT (*i.e.*, ~25 °C), and sample 3 was maintained at body temperature (*i.e.*, ~37.4 °C). Furthermore, under the microscopic (SEM) imaging, sample 2 (stored at RT) gave nanoflowers with surface-functionalized petals and porosity.[19,20] From Fig. 3 and 4, we can see the morphology of the nanoflowers with evenly distributed petals and flakes throughout the capsule surface. Among those, the porosity was also observed in between the inter-petals of the capsule surface. The gaps or inter-petal

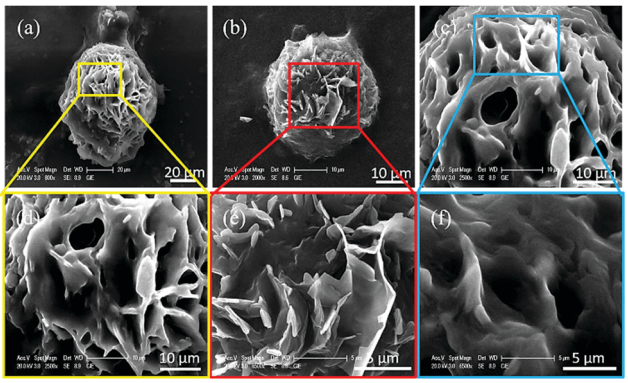

Fig. 3 SEM micrographs (a–c) of NFCs at lower magnifications and (d–f) at higher magnifications. Di-BCP of [(L-GluA-5-BE)-*b*-(L-AspA-4-BE)] was dispersed in propanol, and the sample was maintained at ~25 °C.

distances between the petals and their distribution were shown from the SEM and FESEM micrographs. However, these NFCs with surface-distributed petals were evidenced with various microscopic characterizations. It is worth noting that NFCs with petals are stable and suitable for DDSs.[21] Similarly, sample 3 (maintained at body temperature, *i.e.*, ~37.4 °C) also gave nanoflowers with surface-distributed nanopetals and porosity (Fig. 4). These NFCs are also stable at RT and body temperature. At considerably lower temperatures (8–12 °C), these NFCs are sensitive and show drastic changes in morphology. From Fig. 3 and 4, it is evident that the petals are distributed throughout the capsule surface. From the powder XRD data, the synthesized di-BCP of [(L-GluA-5-BE)-*b*-(L-AspA-4-BE)] solid state was confirmed as amorphous in nature. These amorphous [(L-GluA-5-BE)-*b*-(L-AspA-4-BE)]-based NFCs are highly sensitive to temperature conditions, as well as the concentrations, pH values,

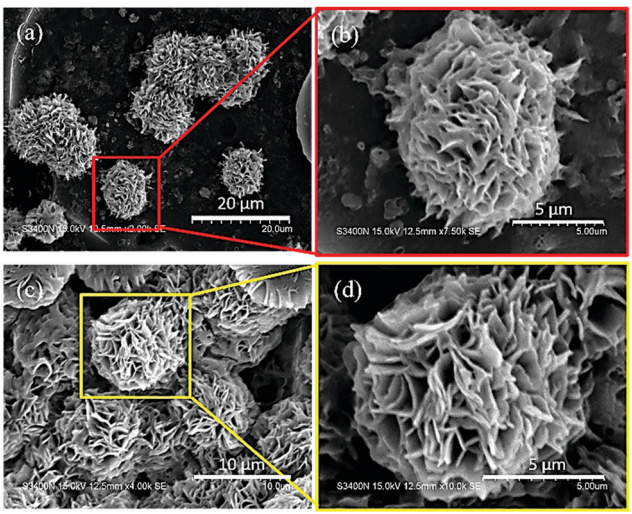

Fig. 4 SEM micrographs (a and c) for NFCs at lower magnifications and (b and d) at higher magnification. Di-BCP of [(L-GluA-5-BE)-*b*-(L-AspA-4-BE)] was dispersed in propanol solvent, and the sample was maintained at ~37.4 °C.

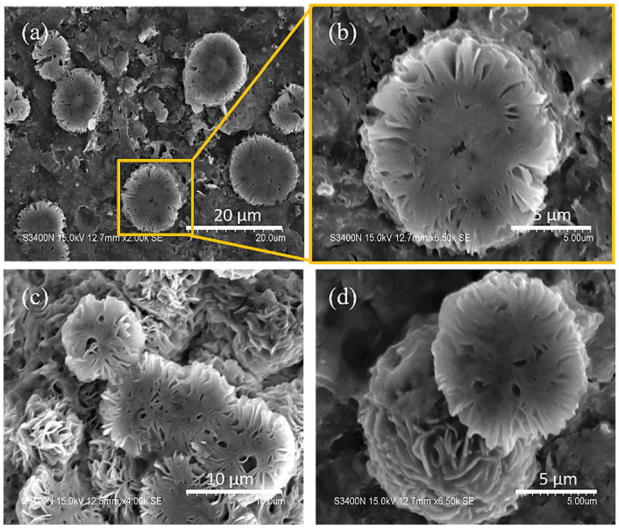

Fig. 5 SEM micrographs (a–d) acquired from lower to higher magnification for disk-type compressed capsules with nanochannels. Propanol-dispersed di-BCP of the [(L-GluA-5-BE)-*b*-(L-AspA-4-BE)] sample was maintained at ~10 °C.

and different solvents.[2,22] From Fig. 3 and 4, the average NFCs size was calculated as ~30 μm (in diameter).

Interestingly, the NFCs (Fig. 3 and 4) are stable at RT and body temperature, which is an advanced characteristic property for consideration as potential cargo for selected drug delivery. However, these NFCs are pH sensitive. Even though the temperature difference is ~12 °C, these NFCs show negligible morphological changes in-between the petal arrangements. In contrast, sample 1 dispersed at lower temperatures, such as 8–10 °C (maintained by using ice-bath), showed a disk-type compressed morphology of the capsules with surface-distributed nanochannels (Fig. 5). However, the nucleation and growth of the nanopetals depend on the dispersion solvent, as well as the temperature of the medium.[23] The surface of the nano-scaled capsules distributed with petals and with unique porosity is a remarkable and promising characteristic property of NFCs for theranostic advancements.[24] These advanced features of NFCs show remarkable drug loading capacity, and are attributed to the significant release (controlled and sustained with precise doses) to malignant organs and tissues through the pH-based release kinetics. Thus, compressed nanochannels can also contribute to loading the drug molecules throughout the surface of the disk-type spherical capsules with certain limitations (Fig. 5). Nanoscale flowers can be a host material to incorporate the drug molecules inside the pores and in-between the petals.[25,26] However, the interaction between the dispersion solvent and di-BCP leads to the growth of micron-sized capsules, along with nanoscale surface-distributed flower-type petals. However, the powder of di-BCP of [(L-GluA-5-BE)-*b*-(L-AspA-4-BE)] was dispersed in propanol solvent, which further nucleated through the self-assembly process between the active functional groups of the polymer (such as ester (R–COOR), hydroxyl (–OH), amide (–NH)). The pi-bonds with larger resonating capacity lead to the

formulation of NFCs. The nanopetal growth and arrangement on the surface of the spherical capsule is very much random, inconsistent, and highly asymmetric. The gaps or inter-petal distances and surface porosity show the significant characteristic feature of the capsule to load the nanomedicines and anticancer drugs for targeted delivery. The main driving force to form NFCs is dependent on the dispersion solvent and the temperature conditions of the medium.[26] Moreover, the affinity and electrostatic interaction between the active functional groups of the synthesized di-BCP of [(L-GluA-5-BE)-*b*-(L-AspA-4-BE)] lead to the formation of NFCs. In addition, the self-assembly process coordinates with the dispersion solvent, followed by the nucleation, which ultimately gives the surface-distributed NFC complexes. When the propanol-dispersed compound is maintained at different temperature conditions, the nucleation growth of the nanopetals takes place for the spherical nanoflower capsules. Thus, it exhibits porosity, which enhances the drug loading capacity. With the change of the dispersion solvent and temperature conditions, the morphology, size, shape, and surface properties might have been changed.[27,28] Through the self-assembly process, the active functional groups tend to show affinity with the dispersion solvent and trigger the nucleation of petals. The amphiphilic nature of di-BCP of [(L-GluA-5-BE)-*b*-(L-AspA-4-BE)] with ionic capacity formulates the spherical shaped NFCs.[28] Furthermore, the amino-acid residues with nitrogen moieties or binding sites tend to contribute to the underlying process to nucleate the petals on the capsule surface.[29] With the increase or decrease of temperature conditions, sample medium results in morphological changes from perfect NFCs to compressed disk-type morphology. These amino-acid-based polymer nanoflower capsules are recommended for many applications, such as catalysis, drug delivery, and analytical science applications.[2,17,29] The hydrophobic and hydrophilic nature of the final compound helps in molecular imprinting to create pores, cavities and voids on the surface of the capsule. There is a need to understand the detailed interface science between the synthesized block copolymer and solvent used for dispersion, along with the temperature effect. The porosity and flake thickness were further characterized with the help of AFM (atomic force microscopy) imaging of non-contact mode operation. Fig. 6 and Fig. S7, S8 (ESI†) show the characteristic features of the surface-functionalized nanocapsules.

The yellow arrows in Fig. 6(a) show the petal thickness, as well as the distances between two particular petals.[17,30] Fig. 6(b) corresponds to the 2D phase(s) of NFCs, and shows a line scan between two petals that depicts the gap between them. Fig. 6(c) corresponds to the 3D image of petals with surface properties and height profiles. Similarly, Fig. 6(d) depicts the surface profile of NFCs with width, depth, and thickness of particular petals on the capsule surface. The gap between those two particular petals (petals 1 and 2) was calculated as 4.2 μm. The average depth of the petals was measured as 21.2 nm.[2,17,31] The design and development of [(L-GluA-5-BE)-*b*-(L-AspA-4-BE)]-based carrier capsules with characteristic surface-functionalized features is a novel approach in the drug delivery fields. It is a

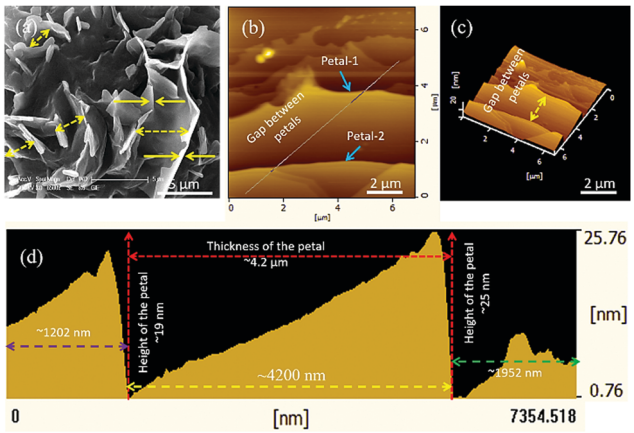

Fig. 6 SEM image (a) depicts the hierarchy of the nanopetals on the NFC surface. AFM image (b) for the phase(s), (c) for the 3D and (d) surface profile of NFCs.

cost-effective and facile method to synthesize the block copolymer of amino-acids, such as [(L-GluA-5-BE)-*b*-(L-AspA-4-BE)]. This synthesized, di-block copolymer plays a crucial role as a potential payload for many anticancer drugs and nanomedicines through the surface-active complexes.[2,29–31] Furthermore, [(L-GluA-5-BE)-*b*-(L-AspA-4-BE)]-based NFCs were characterized through energy-dispersive X-ray spectroscopy (EDAX) for elemental and composition analysis. Fig. S9 (ESI†) corresponds to EDAX, and illustrates the presence of elements in the developed NFCs of di-BCP of [(L-GluA-5-BE)-*b*-(L-AspA-4-BE)]. The inset table in Fig. S9 (ESI†) shows the carbon (C) weight at ~64.55% and atomic at ~72.48%; for oxygen (O), the weight is ~30.39% and atomic is ~25.61%, which were calculated for the designed NFCs.[32] The remaining elements in the inset table, such as sulphur (S) and potassium (K), appeared from a mild amount of impurities present in NFCs. However, the thermal stability (degradation temperature, weight loss and heat flow) of the synthesized di-BCP of [(L-GluA-5-BE)-*b*-(L-AspA-4-BE)] and developed NFCs is an essential property to perform TGA (thermogravimetric analysis), as well as DSC (differential scanning calorimetry). Fig. S10 (ESI†) corresponds to the TGA and DSC for the synthesized di-BCP of [(L-GluA-5-BE)-*b*-(L-AspA-4-BE)]. The plot (a) corresponds to TGA, and shows the spontaneous degradation of the NFCs concerning an increase in temperature from 40 to 200 °C. Similarly, the plot (b) corresponds to DSC, and depicts the exothermic heat flow of the NFCs for the same temperature range. The heating and cooling rates of temperature were adjusted to 10 °C min^{-1}. Such surface-functionalized NFCs were attributed to the good surface area (~12 m^2 g^{-1}), and confinement of the nanomedicines and anticancer drugs for targeted release-based on their thermal stability at body temperature.[4,11,14,33]

Viability assay on [(L-GluA-5-BE)-*b*-(L-AspA-4-BE)] NFCs

The designed NFCs of [(L-GluA-5-BE)-*b*-(L-AspA-4-BE)] were further used to examine the biocompatibility (cell viability) through the MTT assay on cultured cell lines, such as HeLa

(human epithelial cervical carcinoma cells) and HEK293 (human embryonic kidney cells). Concentrations of 1, 5, 10, 15, and 25 μg mL^{-1} [(L-GluA-5-BE)-*b*-(L-AspA-4-BE)] NFCs were mixed with the cell lines. Furthermore, samples were allowed to incubate for 24 h in a CO_2 incubator. Slow agitations, followed by stirring, were performed during the treatment hours. Between these two cell lines, HeLa is the cancerous cell line and HEK293 is the healthy (non-cancerous) cell line used for the cell viability assay. Cultured cell lines of approximately 4×10^3 cells per well were added to NFCs. After 24 h of incubation, the 96-well plate was taken out of the incubator and used for the cell viability study (MTT assay). Fig. 8(a) shows the cell viability of [(L-GluA-5-BE)-*b*-(L-AspA-4-BE)]-based NFCs and the results of their biocompatibility for both cell lines. The cell viability (survival rate) for both cell lines is greater than 98% for the bare NFCs. This demonstrates the suitability and biocompatibility of NFCs for drug delivery systems, as reported by Amgoth *et al.*[2,4,11,14] and Chagala *et al.*[34]

Drug release studies

The designed NFCs of [(L-GluA-5-BE)-*b*-(L-AspA-4-BE)] were further used to load the anticancer drug (PTX) to evaluate the drug-loading and release kinetics. However, PTX loading to [(L-GluA-5-BE)-*b*-(L-AspA-4-BE)]-based NFCs was performed through the incubation of capsules and PTX for 24 h in a CO_2 incubator.[34,35] The incubation was followed by slow stirring for better interactions between NFCs and drug molecules. Furthermore, these drug-loaded NFCs were mixed with HeLa cells to check the cell inhibition according to the release of PTX molecules. Fig. 8(b) shows the UV-Visible characterization, which shows the absorbance of the anticancer drug PTX.[35] The maximum intensity of the excited UV-Visible spectra at ~271 nm corresponds to the highly intense peak of PTX. The absorbance *vs.* wavelength plot shows the difference between the standard PTX plots, as well as PTX released from NFCs. The anticancer drug PTX (~1.0 mg) was dissolved in ~1000 μL of DMSO (dimethyl sulfoxide), and its concentration was calculated as ~0.01 mmol. Interestingly, these designed NFCs showed ~780/1000 ng μg^{-1} loading of PTX (which is equal to 78%).[36] Rough surfaces with surface functionalized nanopetals and porosity are a unique property of the capsule to significantly enhance the loading efficacy.

These [(L-GluA-5-BE)-*b*-(L-AspA-4-BE)]-based NFCs loaded with PTX and void porous space and gaps between petals were accommodated with drug molecules in a host–guest manner. Furthermore, these NFCs were used for drug release kinetics through the membrane bag dialysis methods.[37] However, 14 kDa membrane bags were used for the drug release studies at various pH conditions, as well as two different temperatures (such as RT and body temperature). Furthermore, the PTX release studies were performed in acidic (acetic acid) and neutral (PBS) conditions, and in ammonium hydroxide as the basic medium. From Fig. 7(a), we can see the increased drug release trends from neutral to acidic pH levels at different time intervals (max 24 h). More acidic conditions resulted in greater drug release. When the condition was too acidic, (pH at ~3), a

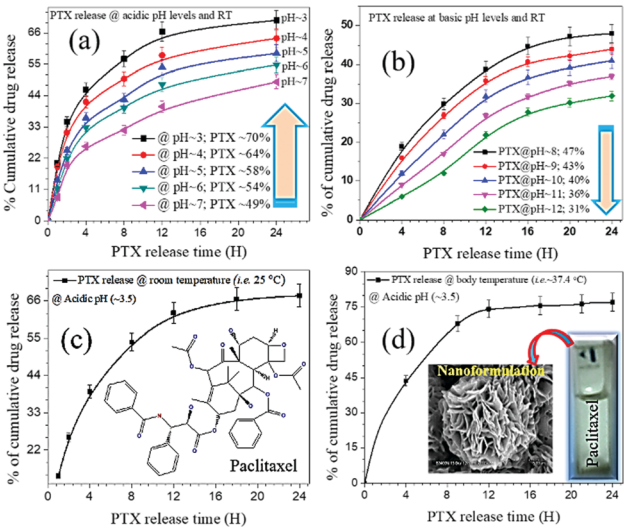

Fig. 7 Plot (a) for cumulative PTX release at acidic pH conditions, (b) for PTX release at basic pH medium, (c) for PTX released at room temperature, and (d) for PTX release at body temperature.

drug release of ~70% was achieved.[4,14,38] As the pH levels gradually increased from 3 to 7, there was a slight decrease in the release of drug molecules (*i.e.*, pH ~ 4 gave 64%, pH ~ 5 gave 58%, pH ~ 6 gave 54% and pH ~ 7 (neutral) gave 49%). Fig. 7(b) shows the percentage of cumulative drug release at basic pH (*i.e.*, ~8, 9, 10, 11 and 12). The PTX release at such basic pH medium showed a decreased trend (like 47, 43, 40, 36 and 31%). Similarly, Fig. 7(c) shows the drug release (68%) at room temperature (RT) with acidic (pH ~ 3.5) medium. Fig. 7(d) shows the PTX release (~74%) at body temperature (*i.e.*, ~37.4 °C) under acidic pH (pH ~ 3.5) medium. The acidic release of PTX at body temperature was greater (~74%) than the release at RT and physiological conditions. The drug release at different pH conditions, as well as at different temperature conditions, was performed through the membrane bag dialysis method followed by slow stirring. During the slow agitations, the incorporated drug molecules came out and passed through the dialysis membrane for the release kinetic studies.[38] The decanted solution of the drugs were used for UV-Visible spectroscopic characterization with different time intervals, and those points were used to draw a cumulative drug release plot. However, these NFCs showed controlled release at different pH values and temperature conditions. It demonstrates the first-order release kinetics, which depends on the concentration and periods with specified dosages.[38,39]

Cell inhibition assay

Furthermore, these potential carrier capsules of [(L-GluA-5-BE)-*b*-(L-AspA-4-BE)] were used to evaluate the cell inhibition studies on cancerous HeLa cells. Fig. 8(c) shows the cell inhibition for bare NFC, free PTX and nanoformulation [(NFCs)-(PTX)]. HeLa cells were used for the *in vitro* cell-based inhibition studies. Based on the MTT assay, the data showed an increased tendency in cell inhibition with an increase of concentration of PTX released from designed NFCs and its effect on cells. Six (6)

different concentrations of PTX (1, 5, 10, 15, 20, and 25 μg mL^{-1}) were separately added to fixed (~4×10^3 cells per well) numbers of HeLa cells in each case, and allowed to incubate for 24 h. The blank column shows zero cell inhibition because of the absence of nanoformulations. For the control, no drug-loaded NFCs were added. Cells as cultured were incubated and used for MTT assay analysis for zero cell inhibition. The rest of the six (6) wells of the 96-well plate were added with nanoformulations. During the incubation, the interactions between the cells and released drug molecules led to the cell inhibition process. The incubation period of 24 h with the nanoformulations and cells was termed as the treatment time before the MTT assay. As the PTX concentration increased from ~1 to 25 μg mL^{-1}, the cellular inhibition also gradually increased.[2,14,39]

~1 μg mL^{-1} concentration of PTX showed ~26% cell inhibition, and ~25 μg mL^{-1} of PTX concentration showed ~79% of inhibition. The bare NFCs showed negligible cell inhibition. From these studies, it is evident that NFCs with surface-functionalized properties showed enhanced drug loading efficacy, as well as the potential release to kill the cancer cells with preferable cell inhibition. These *in vitro* cell-based studies showed that the characteristic properties of the novel carrier capsules of [(L-GluA-5-BE)-*b*-(L-AspA-4-BE)] are predominant for cancer treatment and other biomedical usages through the pH-responsive controlled release kinetics.[37,39] Fig. 8(d) shows the FACS (fluorescence-activated cell-sorting), and quadrant(Q) represents the cell distribution after 24 h treatment with our developed NFC-based nanoformulations. Further, cells killed with various reasons such as mechanical damage, medium (Q1) is measured as 4%, the necrotic cells mechanical damage (Q2) is 8%, Q3 corresponds to the viable cells 56% and apoptotic cells (Q4) corroborates the cells killed with our developed nanoformulations (which means because of PTX released from NFCs) has been calculated as ~34%.

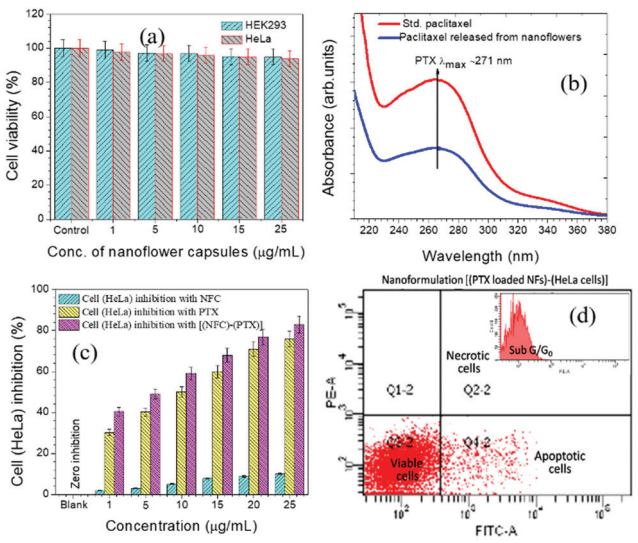

Fig. 8 Plot (a) for cell survival rate, (b) UV-Visible for standard PTX and released PTX from NFCs, (c) for cell inhibition, and (d) for FACS of apoptotic cells.

Apoptosis is a programmed cell-killing process, whereas our [(NFCs)-(PTX)-(HeLa)] showed significant cell killing within the 24 h treatment. Fig. S16(a–d) (ESI†) shows the apoptosis for the cells (HeLa) as cultured, NFCs with HeLa cells, PTX with HeLa cells and nanoformulation of [(NFCs)-(PTX)-(HeLa)] cells.

Tumor-bearing rats and anticancer efficacy studies

Healthy and well-cultured 4–6 weeks grown rats were purchased from Jackson Laboratory, and used for inflammation studies. The tumor growth was observed, and allowed to grow up to 150 to 220 mm^3 size. Rats were then randomly divided into four parts, such as PBS (pH of 7.2 with 0.02 mmol) saline, NFC (500 μg mL^{-1}) dispersed in propanol, NFC–PTX (1 : 1 equimolar ratio of 500 μg mL^{-1}), and PTX (500 μg mL^{-1} dissolved in organic solvent DMSO). Furthermore, drugs were injected subcutaneously, and the tumor growth was illuminated and monitored from day 1 to day 30 (Fig. 9(a)). Similarly, Fig. 9(b) shows the densitometric analysis and expression of COX-2, iNOS by western blot analysis for the control sample and samples with NFC, PTX, and its combination (such as [(NFC)–(PTX)]). The expressions of COX2 and iNOS in tumor tissue were examined by immunohistochemistry, $^*p < 0.05$ *vs.* the NFC groups. Fig. 9(c) shows the tumor volume with respect to time in days with our NFC groups and saline. Fig. 9(d) shows a gradual increase in the body weight of the rats post-treatment. Once the tumor growth reached the optimum size, the tumor growth tissue was extracted, as shown in Fig. 9(a), and was used for anticancer efficacy examinations. The NFC-PTX combination at the same resolution shows the ruptured and fragmented morphology of the cells. Fig. 9(e–h) visually demonstrates the normal tissue structure without any harm (control) and the damage on the inflammatory lesions with NFC, PTX and combined [(NFC)–(PTX)]. From the H and E staining in the tissue treated with [(NFC)–(PTX)], it can be concluded that the developed nanoformulations are promising agents to kill the cancer tumor cells. Furthermore, this was demonstrated with the apoptosis examinations, and the detailed results have been incorporated into the respective sections.

Cell uptake

After the cell inhibition assay, further cell-based studies were performed to examine the morphology of the treated HeLa cells. 0.5 μg of [(L-GluA-5-BE)-*b*-(L-AspA-4-BE)]-based NFCs were dispersed in 2.5 mL of propanol. 1 mg of PTX was dissolved in DMF, and 200 μL of the drug suspension was used to load with NFCs, which were already dispersed in propanol. Finally, those two were mixed through the vigorous stirring methods to load the drug molecules inside the pores and gaps in-between the NFC petals. The drug-loaded NFCs were then added to the wells of the 96-well plate. Each well was filled with a fixed amount of HeLa cells (~4×10^3 cells per well).[2,4,40] The combination of nanoformulation and HeLa cells were allowed to incubate for 24 h under humidified conditions by using CO_2 incubator. Slow agitations were performed to release the PTX molecules from NFCs and interact with HeLa cells, followed by the penetration of the cell membrane. After 24 h of treatment, the wellplate was

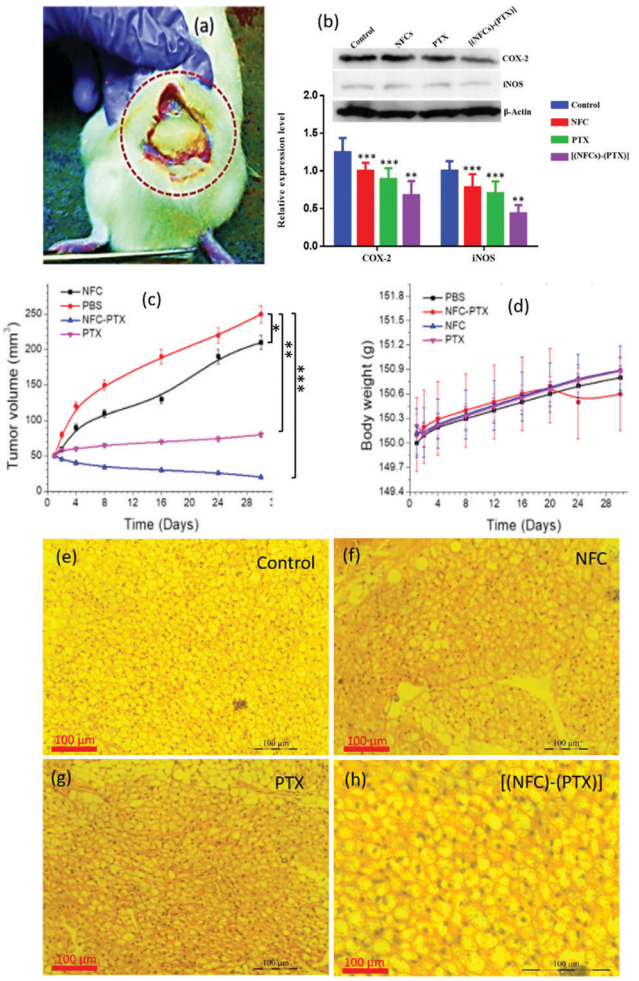

Fig. 9 (a) Normal photograph of rat representing the dissected tumor. (b) Densitometric analysis and expression of COX-2, iNOS by western blot analysis for NFC, PTX and its combination. (c) Tumor volume and (d) rat body weight as a function of time. Microscopic images (e–h) with H and E staining of tumor tissue for the control sample and samples treated with NFC, PTX, and NFC–PTX, respectively. Scale bars were 100 μm.

taken out of the incubator. Imaging was performed by laser scanning confocal microscopy (LSCM).[38–40] Wells were added with different dyes to stains the cell organelles to understand the ruptured morphology of the complete cells. The dyes used for the studies included FITC (fluorescence isothiocyanate), a green fluorescent dye that stains the cell membrane, and DAPI, a blue fluorescent dye (2-(4-aminophenyl)-1*H*-indole-6-carboxamidine), which particularly stains the genetic material (adenine and thymine/A-T) rich regions of the cells. Similarly, rhodamine-B, a red fluorescent dye, was also added to the cells to stain the cell membrane.

The well-stained cell samples were used for confocal microscopic characterization to understand the cellular uptake, followed by the ruptured, swelled, and fragmented morphology of the treated cells. Fig. 10 shows the HeLa cells treated with our developed nanoformulations and the morphology of the cells after 24 h treatment.[40–42] Fig. S11 and S12 (ESI†) show the confocal microscopic images of the HeLa cells that exhibit

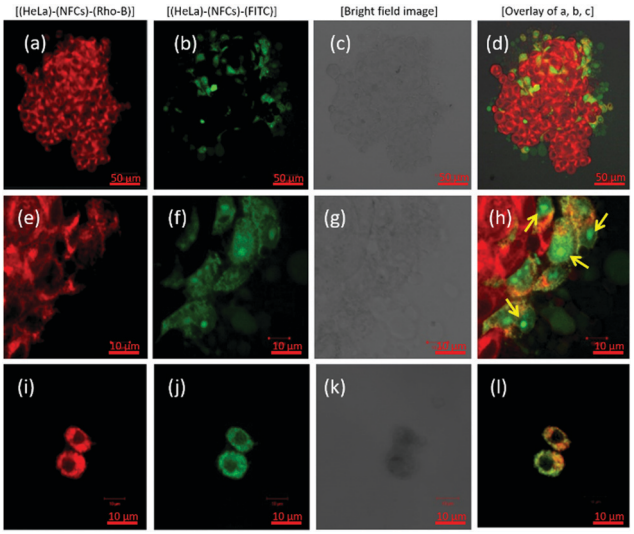

Fig. 10 LSCM images of HeLa (Human epithelial cervical carcinoma) cells. Top to bottom images were acquired from lower to higher magnifications. Cells were captured after 24 h treatment with PTX released from the designed NFCs. Cells were stained with red fluorescent dye Rho-B and green fluorescent dye FITC, followed by their bright field and merged images (right side).

the ruptured, leaky, and fragmented morphology of the cells after treatment with our developed nanoformulations. The yellow arrows in Fig. 10(h) show the nucleus of the cell with the ruptured cell morphology. The aggregate of the ruptured cells was segregated through slow stirring methods to separate the individual cells, as represented in Fig. 10(l), for a better understanding of the treated cells and the cellular uptake of nanomedicines and dye distribution.

Conclusions

In conclusions, we report the simple and facile synthesis of an amino-acid-based di-block copolymer of [(L-GluA-5-BE)-*b*-(L-AspA-4-BE)] between L-glutamic acid-5-benzyl ester and L-aspartic acid-4-benzyl ester. The synthesis was followed by the ring-opening polymerization (ROP) without the use of any surfactants and precursors. Importantly, the synthesized [(L-GluA-5-BE)-*b*-(L-AspA-4-BE)] compound gave NFCs upon dispersion in propanol. Interestingly, [(L-GluA-5-BE)-*b*-(L-AspA-4-BE)] showed the thermosensitive morphology of NFCs at three different temperature conditions, such as low (~10 °C), RT (~25 °C) and body temperature (*i.e.*, ~37 °C). From the SEM micrographs, the sample maintained at lower temperature gave disk-shaped capsules with surface-distributed nanochannels. The samples maintained at RT and body temperature gave NFCs with surface-functionalized nanopetals and porosity. Furthermore, our collective and systemic studies on drug loading and release revealed the unique characteristic property, which is the pH-responsive drug release nature of NFCs. The findings in our study demonstrate the enhanced drug loading capacity (*i.e.*, ~78%; w/w) of NFCs because of the

surface-distributed petals and porosity. Therefore, NFCs deliver the PTX target specifically upon changing the trajectory medium. Our *in vitro* and *in vivo* studies validate NFCs as prominent delivery systems, which stimulate apoptosis to kill the cancer cells. Confocal microscopic images of the cell uptake demonstrate the inherent imaging performance of the treated (HeLa) cells. It explores NFCs as thermosensitive and pH-responsive potential cargo materials for cancer theranostics. Such promising NFCs with remarkable characteristic features can be recommended for catalysis, biosynthesis, and molecular bioimprinting technology. In addition, it is proposed for tissue engineering and other cancer therapeutics.

Author contributions

C. A. performed all of the experiments, including the synthesis of di-BCP and development of NFCs, and wrote the manuscript. S. C. helped with the statistical data analysis. T. M. contributed by performing the MTT assay (cell viability and inhibition) studies. G. T. contributed through the correction of the manuscript and valuable input.

Conflicts of interest

The authors declare that there are no conflicts of interest.

Acknowledgements

The authors would like to acknowledge the Department of Chemistry, Zhejiang University for financial support and research facilities. This work has been jointly supported by the National Natural Sciences Foundation of China (Grant No. 51873185).

Notes and references

1 L. C. Preiss, L. Werber, V. Fischer, S. Hanif, K. Land fester, Y. Mastai and R. M. Espi, *Adv. Mater.*, 2015, **27**, 2728.
2 C. Amgoth, G. Dharmapuri, A. M. Kalle and P. Paik, *Nanotechnology*, 2016, **27**, 125101.
3 A. M. Oliveir, E. Jager, A. Jager, P. Stepanek and F. C. Giacomelli, *Colloids Surf., A*, 2013, **436**, 1092.
4 C. Amgoth, M. Lakavathu and D. S. D. S. Joshi, *Bull. Mater. Sci.*, 2018, **41**, 142.
5 C. Zhang, D. Li, P. Pei, W. Wang, B. Chen, Z. Chu, Z. Zha, X. Yang, J. Wang and H. Qian, *Biomaterials*, 2020, **237**, 119835.
6 C. Amgoth and S. Joshi, *Mater. Res. Express*, 2017, **4**, 105306.
7 R. Ni, G. Song, X. Fu, R. Song, L. Li, W. Pu, J. Gao, J. Hu, Q. Liu, F. He, D. Zhang and G. Huang, *Biomaterials*, 2020, **232**, 119730.
8 D. Li, T. Su, L. Ma, F. Yin, W. Xu, J. Ding and Z. Li, *Eur. J. Med. Chem.*, 2020, **199**, 112367.
9 W. Wu, T. Zhou, A. Berliner, P. Banerjee and S. Zhou, *Chem. Mater.*, 2010, **22**, 1966.
10 K. Wang, Q. Hu, W. Zhu, M. Zhao, Y. Ping and G. Tang, *Adv. Funct. Mater.*, 2015, **25**, 3380.
11 C. Amgoth, A. Singh, R. Santhosh, S. Yumnam, P. Mangla, R. Karthik, T. Guping and M. Banavoth, *RSC Adv.*, 2019, **9**, 33931.
12 J. Ding, J. Chen, L. Gao, Z. Jiang, Y. Zhang, M. Li, Q. Xiao, S. S. Lee and X. Chen, *Nano Today*, 2019, **29**, 100800.
13 W. Wu, Q. Hu, M. Wang, S. Shao, X. Zhao, H. Bai, J. Huang, G. Tang and T. Liang, *Chem. Commun.*, 2019, **55**, 9363.
14 C. Amgoth, S. J. D. S. Doddapaneni, G. Dharmapuri and M. Lakavathu, *Mater. Sci. Eng., C*, 2018, **92**, 790.
15 J. Zhao, Y. Yang, X. Han, C. Liang, J. Liu, X. Song, Z. Ge and Z. Liu, *ACS Appl. Mater. Interfaces*, 2017, **9**, 23555.
16 F. J. C. Bayard, W. Thielemans, D. I. Pritchard, S. W. Paine, S. S. Young, P. Backman, P. Ewing and C. Bosquillon, *J. Controlled Release*, 2013, **171**, 234.
17 J. Ge, J. Lei and R. N. Zare, *Nat. Nanotechnol.*, 2012, **7**, 142.
18 M. A. Quadir, S. W. Morton, Z. J. Deng, K. E. Shopsowitz, R. P. Murphy, T. H. Epps and P. T. Hammond, *Mol. Pharmaceutics*, 2014, **11**, 2420.
19 J. P. Bertram, S. M. Jay, S. R. Hynes, R. Robinson, J. M. Criscione and E. B. Lavik, *Acta Biomater.*, 2009, **5**, 2860.
20 Z. Ge and S. Liu, *Chem. Soc. Rev.*, 2013, **42**, 7289.
21 G. Levi, Y. Scolnik and Y. Mastai, *ACS Appl. Mater. Interfaces*, 2016, **8**, 23356.
22 N. R. Champness, *Dalton Trans.*, 2011, **40**, 10311.
23 C. Dohmen, D. Edinger, T. Frohlich, L. Schreiner, U. Lachelt, C. Troiber, J. Radler, P. Hadwiger, H. P. Vornlocher and E. Wagner, *ACS Nano*, 2012, **6**, 5198.
24 L. Sun, X. Ma, C. M. Dong, B. Zhu and X. Zhu, *Biomacromolecules*, 2012, **13**, 3581.
25 C. Tang, A. F. Miller and A. Saiani, *Int. J. Pharm.*, 2014, **465**, 427.
26 A. M. L. Hossion, M. Bio, G. N. kepang, S. G. Awuah and Y. You, *ACS Med. Chem. Lett.*, 2013, **4**, 124.
27 K. K. Perkin, J. L. Turner, K. L. Wooley and S. Mann, *Nano Lett.*, 2005, **5**, 7.
28 I. R. Fernando, D. P. Ferris, M. Frasconi, D. Malin, E. Strekalova, M. D. Yilmaz, M. W. Ambrogio, M. M. Algaradah, M. P. Hong, X. Chen, M. S. Nassar, Y. Y. Botros, V. L. Cryns and J. F. Stoddart, *Nanoscale*, 2015, **7**, 7178.
29 F. Pan, Z. Lu, I. Tucker, S. Hosking, J. Petkov and J. R. Lu, *J. Colloid Interface Sci.*, 2016, **484**, 125.
30 J. Du, L. Fan and Q. Liu, *Macromolecules*, 2012, **45**, 8275.
31 M. T. Raisanen, A. G. Slater, N. R. Champness and M. Buck, *Chem. Sci.*, 2012, **3**, 84.
32 S. Lv, M. Li, Z. Tang, W. Song, H. Sun, H. Liu and X. Chen, *Acta Biomater.*, 2013, **9**, 9330.
33 N. Bailly, M. Thomas and B. Klumperman, *Biomacromolecules*, 2012, **13**, 4109.
34 Y. E. A. Chagala, J. L. Santos, Y. Huang and M. H. Alonso, *ACS Macro Lett.*, 2014, **3**, 1249.
35 L. Shi, J. Shan, Y. Ju, P. Aikens and R. K. Prudhomme, *Colloids Surf., A*, 2012, **396**, 122.
36 Y. Shao, C. Shi, G. Xu, D. D. Guo and J. Luo, *ACS Appl. Mater. Interfaces*, 2014, **6**, 10381.
37 Q. Chen, H. Bai, W. Wu, G. Huang, Y. Li, M. Wu, G. Tang and Y. Ping, *Nano Lett.*, 2020, **20**, 11.

38 L. Momtazi, S. Bagherifam, G. Singh, A. Hofgaard, M. Hakkarainen, W. R. Glomm, N. Roos, G. M. Malandsmo, G. Griffiths and B. Nystrom, *J. Colloid Interface Sci.*, 2014, **433**, 76.
39 T. Chanlen, S. Hongeng and N. Nasongkla, *J. Polym. Res.*, 2012, **19**, 36.
40 T. Chen, S. Xu, T. Zhao, L. Zhu, D. Wei, Y. Li, H. Zhang and C. Zhao, *ACS Appl. Mater. Interfaces*, 2012, **4**, 5766.
41 J. Liu, L. Xie, J. Deng, Y. Gong, G. Tang, H. Bai and Y. Wang, *Chem. Mater.*, 2019, **31**, 7186.
42 P. Zheng, Y. Liu, J. Chen, W. Xu, G. Li and J. Ding, *Chin. Chem. Lett.*, 2020, **31**, 1178.